Gravity and Magnetic Constraints on the Crustal Structure and Evolution of the Horeki Seamount in the Izu-Bonin Arc

Toshiya Fujiwara[1], Yukari Kido[1], Yoshihiko Tamura[1], and Osamu Ishizuka[2]

Abstract We conducted a multi-beam bathymetry, gravity, and magnetic survey of the Horeki seamount in the Izu-Bonin arc, the western Pacific. On the basis of gravity anomaly, the flanks of the Horeki seamount are consistent with higher density anomaly. On the other hand, low density anomaly is distributed parallel to the long axis in the top part of the seamount. The prominent circular low Bouguer gravity anomaly, appeared in the northern part of flat-topped summit, indicates light density material filling the flat-topped summit. From the aspect of magnetic anomaly, the main body of the seamount is magnetized in positive. The magnetization indicates the volcanism constructed the main body is most robust in Gauss normal magnetic epoch (3.6-2.6 Ma). The negative magnetization is in the eastern part of the small ridges located to the north of the seamount, therefore the volcanism of these ridges is estimated to be active in Matuyama reverse epoch (2.6-0.8 Ma). In contrast, the western part of the northern ridges is magnetized in positive, and suggested to be constructed in Brunhes normal epoch. The southern part of the seamount flanks, where small volcanic cones are well developed, is magnetized in slightly positive with low magnitude. The remnant magnetization of the seamount flanks may be nearly canceled each other out by the small cone's magnetization. These volcanic cones may have erupted in various ages or in different epoch from the seamount's main body.

Keywords: Izu-Bonin arc; Horeki seamount; gravity anomaly; magnetic anomaly; crustal structure.

1. Introduction

The Izu-Bonin arc is an active, ~1200 km long, intra-oceanic arc associated with the Pacific-Philippine Sea plate convergence, in the western Pacific (Figure 1). The Izu-Bonin arc is one of the best to study intra-oceanic arc evolution and continental crust formation, because the Izu-Bonin is a juvenile arc, the tectonic evolution is better known, and the arc is the best-surveyed intra-oceanic arc.

Recently, a research group in IFREE, JAMSTEC, in collaboration with other Japanese and overseas institutions, has been extensively conducted geological and geophysical surveys. As for the geophysical surveys, whole crustal scale seismic experiments have been conducted, and several profiles of the crustal structure along and across the arc are obtained [e.g. Park et al., 2002; Takahashi et al., 2005; Tsuru et al., 2005; Kaiho et al., 2006; Miura et al., 2006; Nishizawa et al., 2006]. Meanwhile, detailed surveys of multibeam bathymetry, gravity, magnetics, and seismics around dredge sites or submersible/ROV diving sites also have been carried out [e.g. Kido, 2005].

In this paper, we present gravity and magnetic data of the Horeki seamount in the Izu-Bonin arc collected during underway geophysical survey aboard R/V *Kairei* (cruise ID: KR04-04) conducted in 2004. We expect that our geophysical survey and an integration of these results will provide data necessary to assess magma genesis, crustal evolution and their variation along and across the whole arc.

2. Geological Setting

The Horeki seamount is a back-arc seamount located ~100 km west-southwest of the Torishima island (situated on the volcanic front) in the northern Izu-Bonin arc (Figure 1). Detailed bathymetry has become visible as the result of our survey in 2004 (Figure 2). At the depth of 1800-2000 m, the main body of Horeki has an elliptical base of ~25 km long and 15 km wide. The seamount elongates in NNE-SSW. The summit with a depth of 400-700 m, thus the seamount is ~1500 m in relative height, is flat that is 10 km long and 5 km wide.

1 Institute for Research on Earth Evolution (IFREE), Japan Agency for Marine-Earth Science and Technology (JAMSTEC), Yokosuka 237-0061, Japan

2 Geological Survey of Japan, National Institute of Advanced Industrial Science and Technology (AIST), Tsukuba 305-8567, Japan

Topographic linearments with steps, suggesting faults, are found on the summit area. The seamount has many satellite cones or knolls, especially on its northern and southern flanks. The northern knolls form parallel ridges trending from NNE to SSW, and southern cones are distributed radially from the center of the main body.

Rock samples were collected by dredge and ROV *Hyper-Dolphin* (white circles, Figure 3). Basaltic and andesitic rocks are the main component of the Horeki seamount as far as analysis of the sampled rocks. Basalts from the main body are medium-K and indicate arc-like feature. On the other hand, basalts from the north ridges and the southern lateral cones are low-K and show MORB-like (BABB) feature [Tamura et al., 2006].

K-Ar study of the sampled rocks indicates ages of the main body of the seamount are ~3.6-3.0 Ma (Figure 3). Other ridges and cones have younger ages of ~3.0-2.0

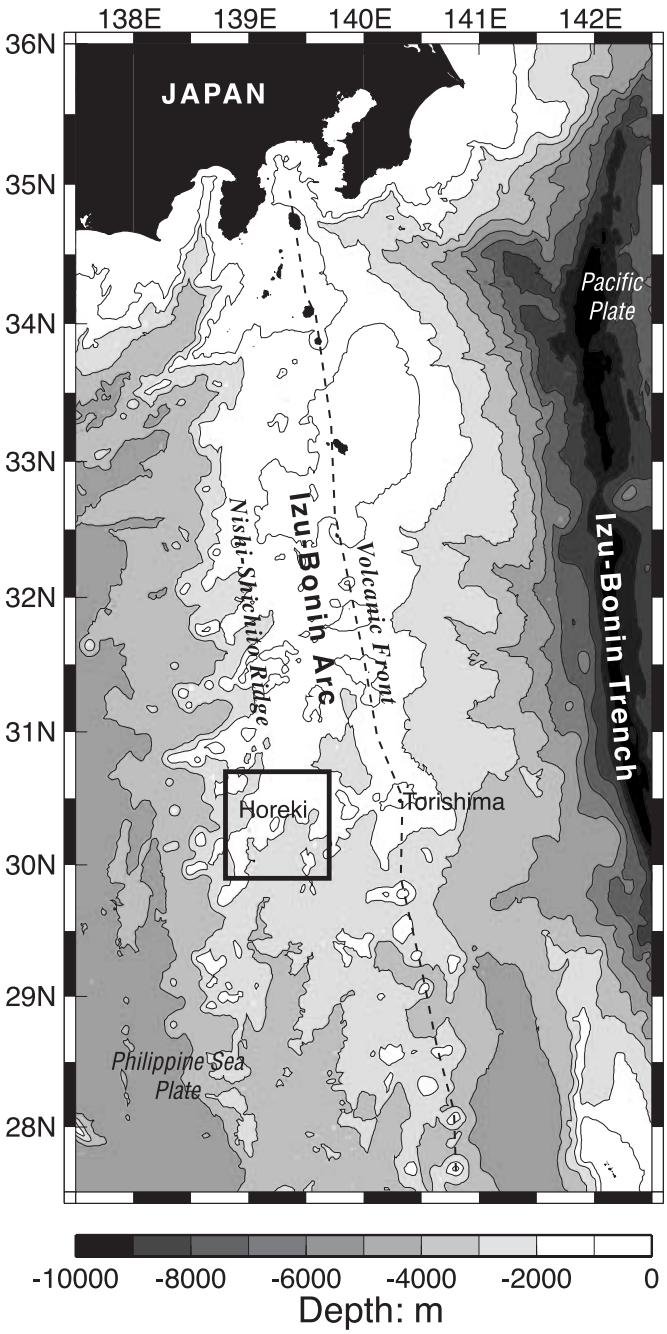

Figure 1: Bathymetry of the northern Izu-Bonin arc showing the location of the Horeki seamount. The black square shows the survey area.

Ma or 0.5 Ma [Ishizuka, unpublished data, 2006].

A multi-channel seismic (MCS) line of KR02-05 cruise crosses over the northern portion of the seamount [Park et al., 2002] (white line, Figure 3). Structure of deep inside the seamount is not evident because of acoustically opaque and multiple reflections. The MCS seismic reflection shows sedimentary basins in the west and east of the seamount. The thickness of the sedimentary basins is estimated to be 0.6-0.8 km and 0.8-1.0 km, respectively.

A refraction seismic survey with ocean bottom seismometers (OBSs) on the same line as MCS line depicts velocity structure of the typical island arc crust with thickness of ~20 km in this portion [Nishizawa et al., 2006]. To reveal the internal structure of the seamount, interval of the OBSs there was rather sparse (>20 km) and also no OBS was deployed on the seamount.

3. Data Collection

3.1 Multibeam Bathymetry

Bathymetric data were obtained using a SeaBeam 2112 multi-narrow beam echo sounder system. Main survey tracks aligned in the north-south direction with a spacing of 3 miles (~4.8 km) (blue lines, Figure 3). The survey covered an area of 80 km in the north-south direction and 50 km in the east-west direction centered at the Horeki seamount.

3.2 Gravity

Onboard gravity measurements were made using a Bodenseewerke KSS-31 marine gravity meter. Gravity data were collected throughout the cruise. The data were

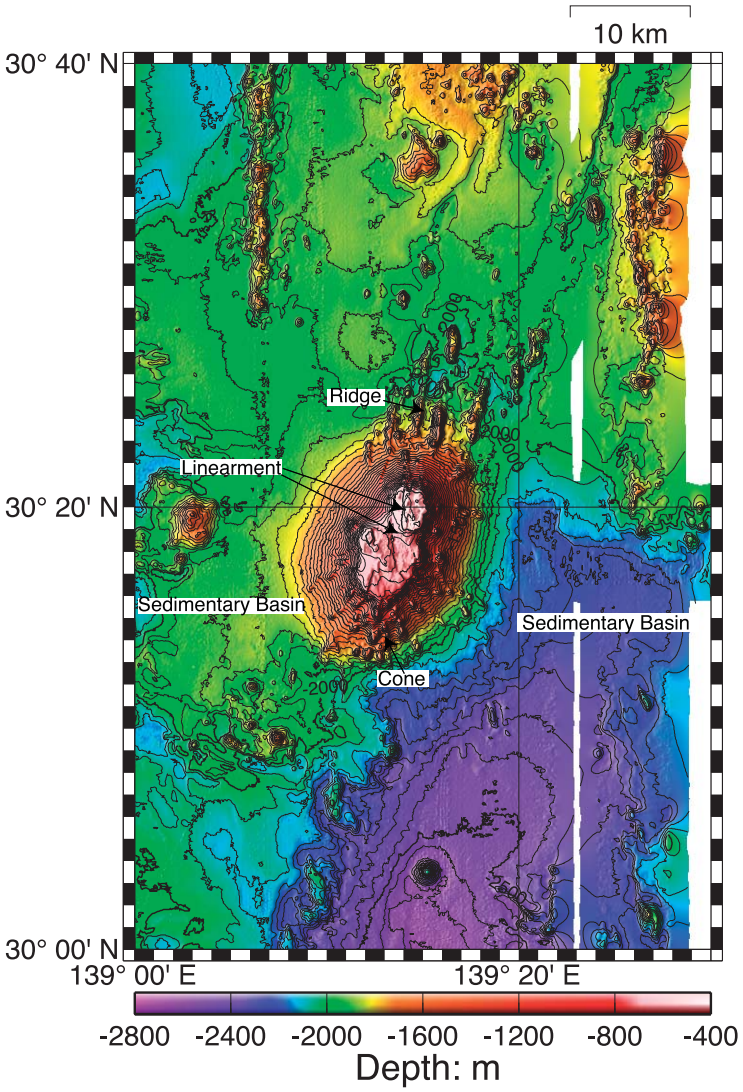

Figure 2: Detailed bathymetry of the Horeki seamount. Contour interval is 50 m.

recorded every 1 minute and survey ship speed was 10 knots, thus, data spacing along ship tracks yielded ~300 m (blue lines, Figure 3).

The gravity meter system incorporates ship's position, speed, and heading through onboard LAN. "Sea State 2" filtering (low-pass filtering to cancel out gravity effect by ship's movement) was selected in the cruise. According to "Sea State" filter, the gravity data output delays 76 seconds. After adjusting the time delay between gravity and navigation data, erroneous data were removed by examining Eötvös correction greater than 3 mGal/min, ship speed slower than 4 kt, and abrupt gravity change greater than 10 mGal/km (4 mGal/min).

The measured gravity value (-1434.3 mGal) was tied to an absolute gravity value at the JAMSTEC pier in Yokosuka (979758.7 mGal). Free-air gravity anomaly was calculated by subtracting from the corrected data the theoretical gravity formula of the Geodetic Reference System 1967 [International Association of Geodesy (IAG), 1967] (Figure 3). Crossover errors at 81 track crossing points in this cruise yielded an RMS standard deviation of 2.2 mGal.

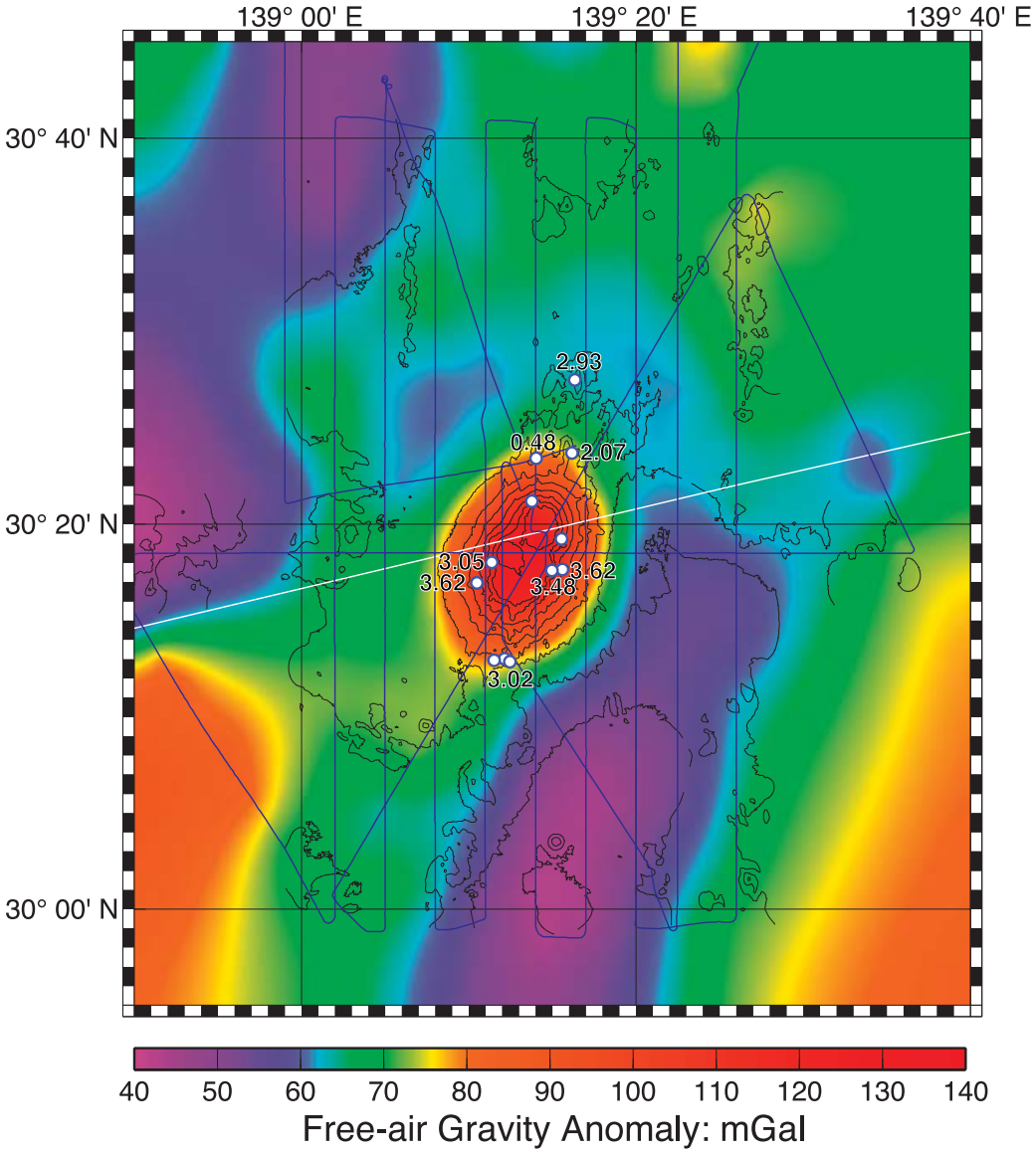

Figure 3: Colored image of free-air gravity anomaly of the Horeki seamount. Black contour lines delineate bathymetry with 200 m intervals. Blue and white lines show survey ship tracks of KR04-04 and a multi-channel seismic (MCS) line of KR02-05, respectively. White circles show rock sample locations. Attached numbers indicate their rock ages in Ma [Ishizuka, unpublished data, 2006].

3.3 Magnetics

Geomagnetic total force data were obtained by using a surface-towed proton precession magnetometer PROTO10 (Kawasaki Geol. Eng. Co.). The sensor was towed 300 m behind the ship. The data were collected every 20 seconds, thus, the data were collected with a spacing of ~100 m along ship tracks (blue lines, Figure 3). After positioning correction taking into account the sensor cable length, the geomagnetic total force anomaly was calculated by subtracting the International Geomagnetic Reference Field (IGRF) 9th generation [International Association of Geomagnetism and Aeronomy (IAGA), 2003] as a reference field (Figure 4). Crossover errors at 46 track crossing points in this cruise yielded an RMS standard deviation of 13.9 nT.

4. Data Analyses

4.1 Density/Magnetization Modelling

We performed density/magnetization modelling mainly reflects the general distribution of density/magnetization near the seafloor, since no strong geological or geophysical constraint on depth distribution of density/magnetization beneath the Horeki seamount is available. Analysis of the density/magnetization structure was accomplished by using inversion of the gravity/magnetic anomalies. A crustal model is com-

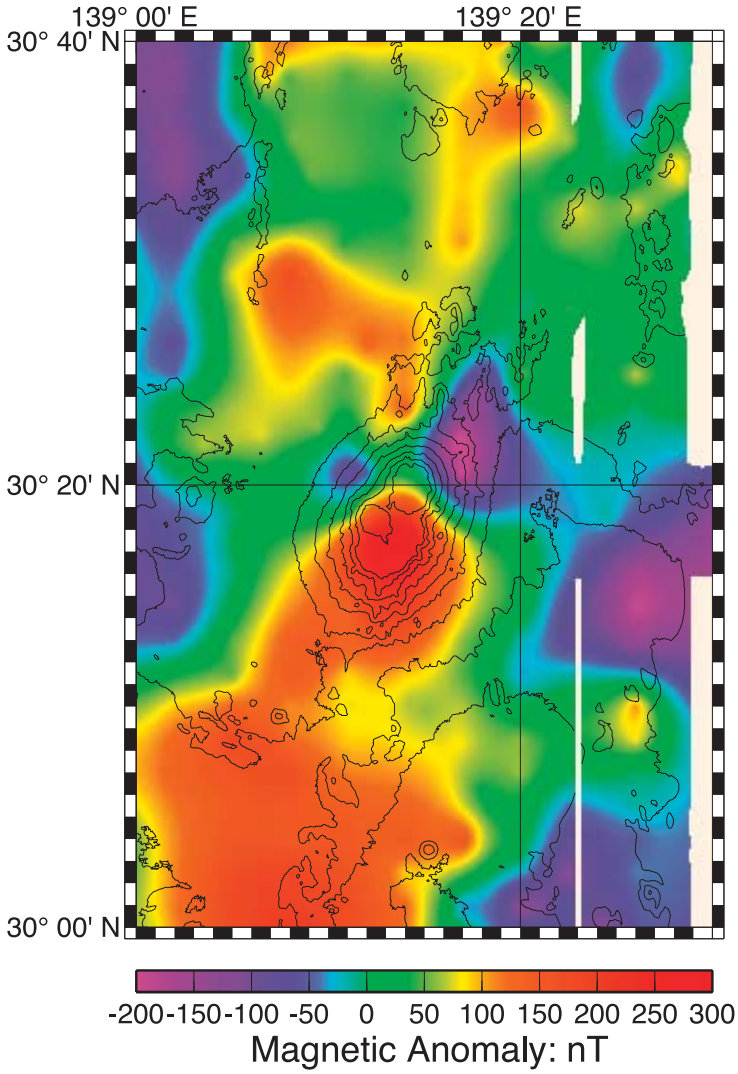

Figure 4: Colored image of magnetic anomaly of the Horeki seamount. Black contour lines delineate bathymetry with 200 m intervals.

posed of a set of prism-shaped bodies as shown in Figure 5. The calculated gravity/magnetic anomaly can be written in matrix form as

$$\mathbf{F} = \mathbf{G} \bullet \mathbf{m} \quad (1)$$

where the bold dot denotes matrix multiplication, **F** and **m** are calculated gravity/magnetic anomalies and density/magnetization written as column vectors, respectively, and **G** is a matrix concerned with the geometric relation between the observation points and prisms. The elements in G can be calculated by using a formulation of Bhattacharyya [1964] and Blakely [1996].

In the case shown in Figure 5, Equation (1) becomes a set of linear algebraic equations:

$$\mathbf{F}_i = \mathbf{G}_{ij} \bullet \mathbf{m}_j \quad (i = 1, 2,..., N; j = 1, 2,..., M) \quad (2)$$

where N is the total number of observations and M is the total number of prism-shaped bodies. The unknown $\mathbf{m}_j$ can be inverted by solving the least squares problem under the condition of $N > M$. A technique of singular value decomposition is applied to solve Equation (2) [Press et al., 1992].

Observed gravity/magnetic data were gridded at 0.5 km spacing for the inversion. Unit prism was also 0.5 × 0.5 km in horizontal extent. Each prism has uniform density or magnetization from surface to the depth. In the inversion, the model prisms were clustered 2.5 × 2.5 km or 1.5 × 1.5 km in horizontal extent according to the spatial resolution of gravity/magnetic anomalies that depends on the water depth and the ship track configuration. As for the upper and lower face undulation, 0.5 km-grid topography was taken into account. High-cut filtering by weighted mean was operated to suppress high frequency oscillation in an ill-conditioned case.

Successively, boundary lines for the prism clustering were modified the locations, and mj was corrected by solving the following equation.

$$\mathbf{d}_i = \mathbf{G}_{ij} \bullet \Delta\mathbf{m}_j \quad (i = 1, 2,..., N; j = 1, 2,..., M) \quad (3)$$

where $\mathbf{d}_i$ is residual between observed gravity/magnetic anomalies and calculated anomalies using the previous model, and $\Delta\mathbf{m}_j$ is correction of density/magnetization. Therefore the final solution was achieved by this iteration process. Note that the calculation areas were broader than areas shown in resultant figures in later sections to avoid side effects from actual sources surrounding the areas.

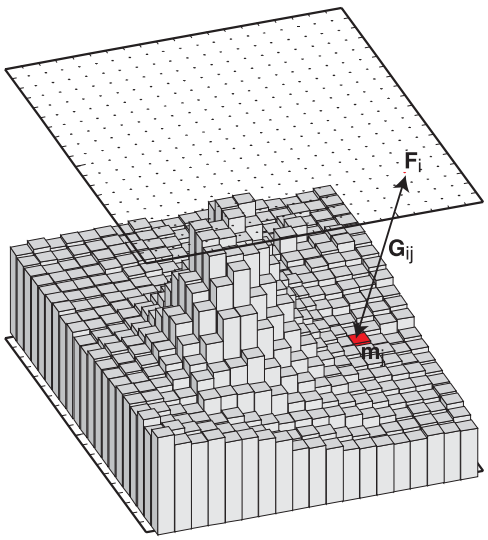

Figure 5: Schematic illustration of the model used in the inversion analysis. Crust is modeled as a set of prism-shaped bodies. Their upper faces follow the seafloor. The bottom depth can be assumed to be any shape.

4.2 Gravity

To examine sub-seafloor density variations, we calculated Bouguer gravity anomaly using the method of Kuo and Forsyth [1988], Prince and Forsyth [1988], and Lin et al. [1990] by subtracting from free-air gravity the predicted gravity effects of seafloor topography. The observed free-air gravity anomaly data were merged with the gravity anomaly data derived from satellite data [Sandwell and Smith, 1997] to extend coverage to areas where no shipboard gravity data were available. And also, to fill unsurveyed area, JTOPO30 topography was merged with. Note that the extended area is not included in interpretations. The topography was gridded at ~180 m for the calculation. To avoid artificial edge effects, we mirrored the grid both east-west and north-south. Assumed density for the gravity calculation was estimated using a G-H (gravity-water depth) correlation method. As the result, calculated Bouguer gravity anomaly with the assumed density of 2510 kg/m^3 gives least correlation with topography in the area around the seamount (30 × 30 km) (Figure 6(a)).

To a first order, long-wavelength Bouguer gravity anomaly reflects variation of crustal thickness of the Izu-Bonin arc [e.g. Ueda, 1996; Geological Survey of Japan, 2000; Fujiwara, 2004]. The gravity anomaly value gradually increases from north to south in accordance with the crustal thickness decreasing. Recent seismic refraction surveys confirm the thickness variation [Kodaira et al., 2006]. The long-wavelength variation of

the gravity anomaly was removed by a linear trend approximation. The residual gravity anomaly is supposed to be caused by sub-surface structure of the Horeki seamount (Figure 6(b)).

The flanks of the seamount are associated with high residual gravity anomaly up to ~5-10 mGal in amplitude compared with a level (Figure 6(b)). In contrast, low anomaly extends parallel to the long axis (NNE-SSW) in the top part of seamount. A prominent feature is circular low anomaly less than 15 mGal in amplitude appeared in the northern part of flat-topped summit. Slight circular low anomaly is also found in the central part of flat-topped summit. The sedimentary basins situated in the western and eastern bases of the seamount are accompanied by low anomaly with amplitude of about -5 mGal.

As for parameters of the gravity inversion, bottom of the model layer was set to have a constant thickness of 1 km, which depth was nearly corresponding to thickness of the sedimentary basins [Park et al., 2002; Nishizawa et al., 2006]. The assumption of the layer thickness may be inappropriate in some places. The choice of another layer thickness would result in different density amplitudes but would not significantly affect the density distribution.

4.3 Magnetics

Long-wavelength positive anomaly is extending in the north-south direction (Figure 4). The long-wavelength anomaly extending along the Nishi-Shichito ridge (the western fringe of the arc) may be due to deeper sources [e.g. Yamazaki and Yuasa, 1998]. Short-wavelength anomalies probably caused by the Horeki seamount are superimposed on the long-wavelength anomaly. The short-wavelength anomalies are dipole-like, which is a pair of anomaly in positive in the south and negative to the north. Amplitude of peak to trough of the dipole anomaly is ~500 nT. The peak is sitting on the seamount and the trough is located on the northeast to the seamount.

In terms of parameters in the magnetic inversion, because the seamount has been formed recently since 3 Ma, no significant drift and rotation of the seamount, associated with the evolution of the northern Izu-Bonin

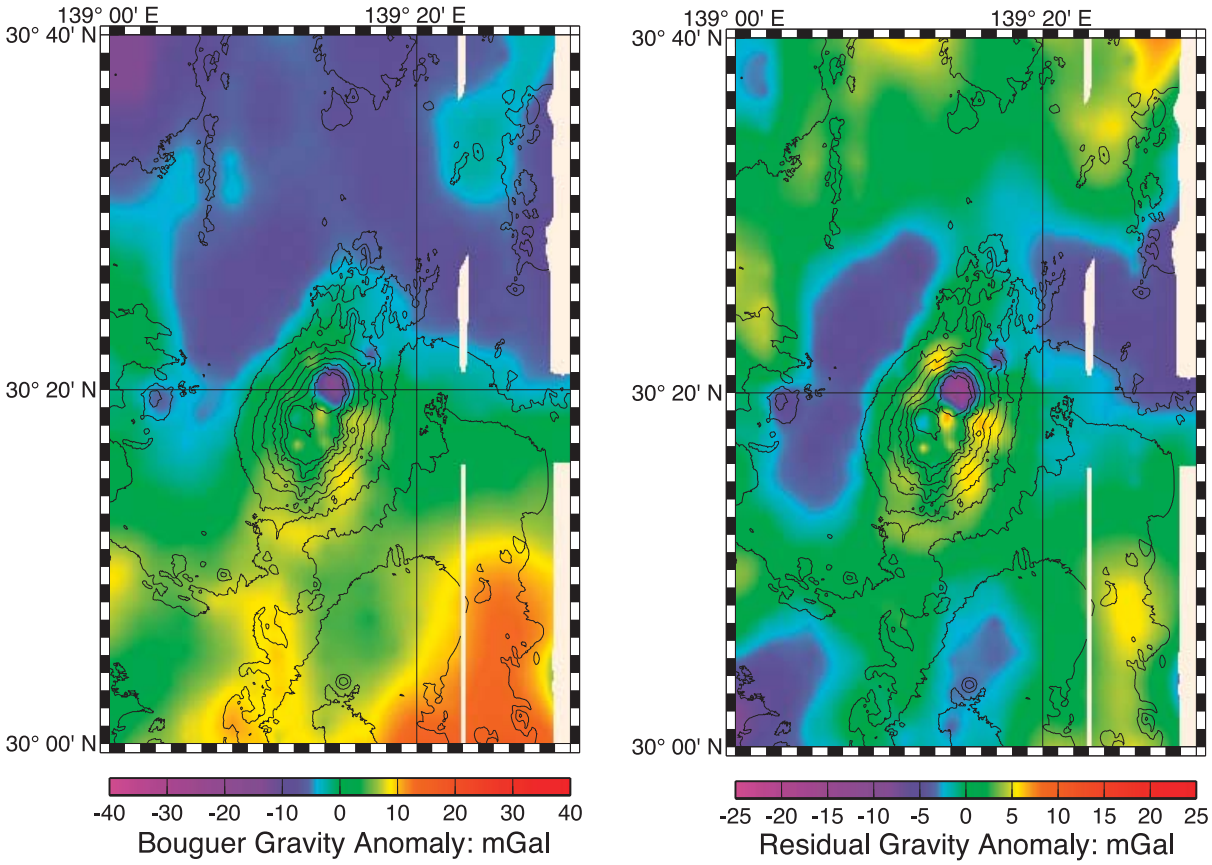

Figure 6: (a) Colored image of Bouguer gravity anomaly of the Horeki seamount. Black lines show topographic contours that outline the seamount, (b) residual Bouguer gravity anomaly.

arc, is expected [Koyama et al., 1992]. Thus, the direction of magnetization in the source layer was reasonably assumed to be oriented parallel to a geocentric dipole field at the present latitude (declination 0°, inclination 49°). The ambient geomagnetic field was set to declination of -5° and inclination of 42° referring to IGRF. A bandpass filter with cosine taper for wavelengths between 40-80 km removed the long-wavelength magnetic anomaly. The bottom depth for the magnetization model corresponds to be 2 km from the seafloor, though it can be assumed to be any shape. In our case, the magnetic anomaly are obtained above the 2000 m water depth, and the effect of sources at 2 km below the seafloor is much smaller than that of surface sources. Therefore, even if we selected a thicker vertical size for the assumed sources in the analysis, the result would differ slightly.

5. Results and Discussion

5.1 Density Structure

Calculated density structure is shown in Figure 7. The colors indicate density difference from the assumed density of 2510 kg/m^3 for the calculation of Bouguer gravity anomaly. The flanks of the seamount are consistent with higher density anomaly. The resultant density exceeds 3000 kg/m^3 in some places of the flanks. However, even dense basaltic rocks have less density than 3000 kg/m^3, and porous basaltic lavas commonly composing a seamount body have much lower density. Therefore, this result of much higher density suggests that assumed thickness of the model is underestimated in such places. The high density anomaly in the seamount flanks can be extended deeper than the assumed thickness of 1 km.

Low density anomaly is distributed parallel to the long axis in the top part of seamount. The resultant density is equal to or slightly lower than the assumed density. The degree of density would be consistent with the andesitic-basaltic rock's density of 2700-2800 kg/m^3 in consideration of more or less ~10 % porosity. Incidentally, mean density of the basaltic rock samples was 2.77 g/cm^3 (2770 kg/m^3), though only a few rocks were measured.

It is possible that volcanic lavas erupted in shallow

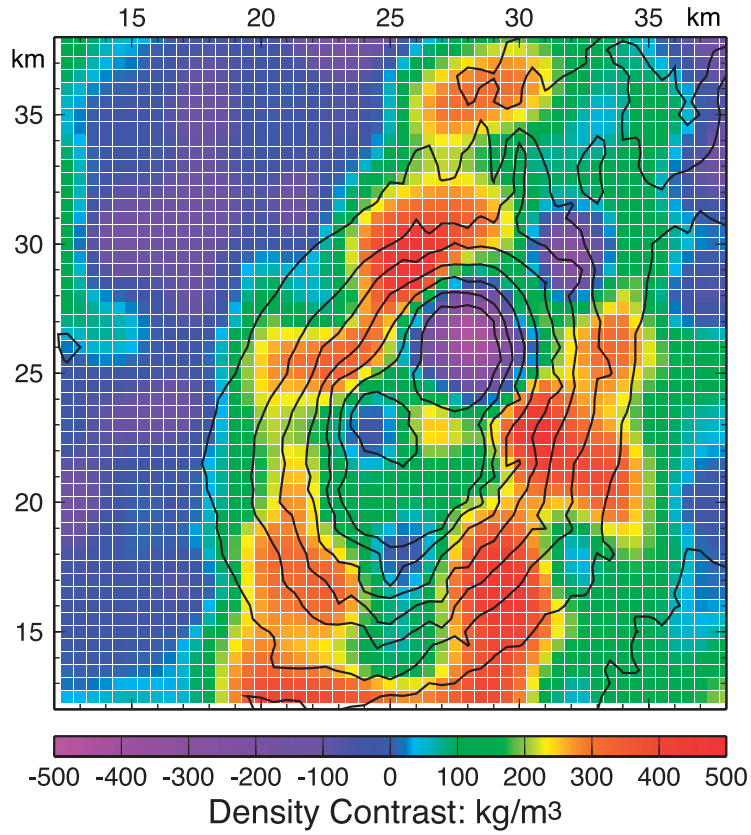

Figure 7: Colored image of density structure of the Horeki seamount. The colors indicate density difference from the assumed density of 2510 kg/m^3. The colored tiles show architecture of prism models with 0.5 × 0.5 km in horizontal extent. Solid lines show 200 m bathymetric contours and outline the Horeki seamount.

water depths tend to have higher porosity, thus tend to be lower density, than lavas erupted in greater depths, because pressure from the weight of the water against the gas pressure in the magma is smaller in the shallow depths. The degree of porosity might be origin of the density structure, which is high density anomaly of the flanks of the seamount in deeper depths and low density anomaly in the top part of seamount.

The prominent circular low anomaly appeared in the northern part of flat-topped summit requires light density material filling the flat-topped summit. The density of the light material caused the low gravity anomaly should be lower by comparison with material filling the sedimentary basins circum the seamount, as discussed later.

The circular shape of the density anomaly on the flat-topped seamount may suggest a guyot that the summit has been above the sea level in previous times. At the certain period, the top of the seamount was planed by waves, and light material deposition such as coral reef formation, piling up of phosphate rocks, and/or other was occurred.

Caldera is also a probable cause of the circular low anomaly. Sub-aqueous volcanoes can make volcanic ash if they reach shallow water depths, and the ash fills the caldera floor. Though, this interpretation contradicts a known tendency of basaltic volcanoes. Calderas and also long axes, which is possible direction of fissure eruptions, of basaltic volcanoes are commonly associated with high gravity anomalies because dense lava flows fill the caldera floors and dike swarms intrude in the fissures, respectively. In any case, there is no strong geological or seismological evidence to constrain the material and the vertical extent yet, although a seismic reflector might be indicated at 0.15 sec two-way travel time beneath the flat-topped summit.

Low density anomalies are consistent with the sedimentary basins. The sedimentary basins deduced from MCS result are landslide deposits (made of volcanic lava) [Park et al., 2002].

5.2 Magnetization Structure

Calculated crustal magnetization is shown in Figure 8. The main body of seamount is magnetized in positive. Magnitude of the magnetization associated with the

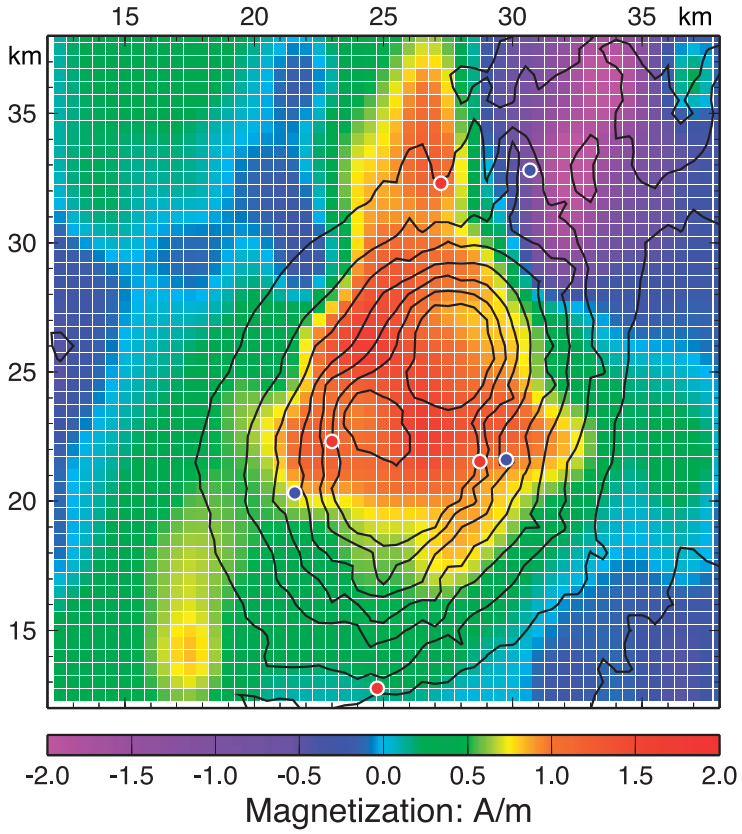

Figure 8: Colored image of crustal magnetization of the Horeki seamount. The colored tiles show architecture of prism models with 0.5 × 0.5 km in horizontal extent. Red and blue circles denote rock sampling locations. Red and blue colors suggest that the rocks are inferred to be erupted in normal and reverse geomagnetic polarities, respectively. Solid lines show 200 m bathymetric contours and outline the Horeki seamount.

seamount body is notably small considering that extrusive volcanic lavas are the source of the magnetic anomaly. In fact, although only a few measurements were made, natural remnant magnetization (NRM) of basaltic lava was 11.2 A/m collected at the northernmost sampling location shown in Figure 8.

The resultant magnetization could be an average of each magnetized layer to the depth direction. Each layer has NRM acquired when erupted and induced magnetization (positive magnetization). The seamount consists of volcanic lavas erupted in various ages. The volcanic lavas erupted in a different magnetic epoch in history, thus obtained NRM of opposite magnetic polarity, cancel the magnetization each other out. As the result, lower magnitude in magnetization will be produced in the model we adopted, assuming uniform magnetization.

Eruption ages of the Horeki seamount range over four major magnetic epochs starting from Gilbert (reverse polarity), Gauss (normal), Matuyama (reverse), to Brunhes (normal) [Gradstein et al., 2004]. The main body of the seamount is probably constructed in Gilbert (5.9-3.6 Ma) and Gauss (3.6-2.6 Ma), according to age analysis [Ishizuka, unpublished data, 2006] (Figures 3 and 8). The resultant (average) positive magnetization indicates the volcanism constructed the main body is more robust in Gauss normal magnetic epoch.

In contrast, negative magnetization overcomes in the eastern part of the northern ridges. The magnetization is consistent with the rock's age obtained from the ridge in this part, therefore the volcanism of these ridges is estimated to be active in Matuyama epoch (2.6-0.8 Ma). From the western part of the northern ridges, young rock's age is obtained (0.48 Ma, Figure 3). In this part, consistently positive magnetization is evaluated (Brunhes epoch: 0.8 Ma-present).

The southern part of seamount flanks, where small volcanic cones are well developed, is magnetized in rather positive with low magnitude. Only one age evidence is obtained from one of the small cones, and the age is in Gauss epoch (Figures 3 and 8). A number of volcanic cones may have erupted evenly in various ages, resulting in randomization of the natural remnant magnetization. Or many of the cones may have erupted in Matuyama epoch and nearly cancel the magnetization of the main body constructed in Gauss epoch.

6. Conclusions

We conducted a multi-beam bathymetry, gravity, and magnetic survey of the Horeki seamount in the Izu-Bonin arc, the western Pacific as a part of the comprehensive research of this arc carried by the IFREE, JAMSTEC. Our analysis of these data yielded the following results:

1. The flanks of the Horeki seamount are consistent with higher density anomaly than the assumed density of 2510 kg/m^3 for Bouguer correction.

2. Low density anomaly is distributed parallel to the long axis in the top part of the Horeki seamount. The resultant density is equal to or slightly lower than the assumed density.

3. The prominent circular low Bouguer gravity anomaly appeared in the northern part of flat-topped summit. Rather light density material filling the flat-topped summit is required.

4. The main body of the Horeki seamount is magnetized in positive. The resultant magnitude of magnetization is attenuated by the volcanic lavas erupted in a different magnetic epoch in history, thus obtained NRM of opposite magnetic polarity. The magnetization indicates the volcanism constructed the main body is more robust in Gauss normal magnetic epoch (3.6-2.6 Ma).

5. The negative magnetization is consistent with the rock's age obtained from the eastern part of the northern ridges, therefore the volcanism of these ridges is estimated to be active in Matuyama epoch (2.6-0.8 Ma).

6. The western part of the northern ridges is magnetized in positive, consistent with the sampled rock's age of 0.48 Ma (Brunhes epoch: 0.8 Ma-present).

7. The southern part of the Horeki seamount flanks, where small volcanic cones are well developed, is magnetized in slightly positive with low magnitude. The remnant magnetization in the southern flanks may be randomized or nearly canceled each other out, because these volcanic cones may have erupted in various ages or in different epoch from the main body.

7. Acknowledgement

We are grateful to the officers and crew of R/V Kairei for outstanding professionalism and dedication that made the cruise successful. We thank the KR04-04 scientific party for collaboration and discussion. We are indebted to marine technicians from Nippon Marine Enterprises and Marine Works Japan for their invaluable help at sea. We thank A. Nishizawa for discussion regarding the KR02-05 OBS survey and N. Takahashi, K. Takizawa, and J.-O. Park for discussion regarding the KR02-05 MCS profile. Bathymetric data of JTOPO30 published by Marine Information Research Center, Japan Hydrographic Association were used to fill unsurveyed area. The GMT software [Wessel and Smith, 1995] was extensively used in this study. Part of this work is a contribution of the research program at the IFREE, JAMSTEC.

References

1) Bhattacharyya, B. K., Magnetic anomalies due to prism-shaped bodies with arbitrary polarization, Geophysics, 29, 517-531, 1964.
2) Blakely, R. J., Potential theory in gravity & magnetic applications, Cambridge University Press, New York, 441 pp, 1996..
3) Fujiwara, T., Gravity anomaly of the Izu-Bonin Island Arc, Eos Trans. AGU, 85(28), West. Pac. Geophys. Meet. Suppl., Abstract V33C-01, 2004.
4) Geological Survey of Japan and Coordinating Committee for Coastal and Offshore Geoscience Programs in East and Southeast Asia, Magnetic anomaly map of east Asia 1:4,000,000 CD-ROM version, 1996.
5) Gradstein, F. M., J. G. Ogg, and A. G. Smith, A geological time scale 2004, Cambridge University Press, United Kingdom, 589 pp, 2004.
6) International Association of Geodesy (IAG), Geodetic Reference System 1967, Bureau Central de A. I. G. Spec. Pub. 3, 1967.
7) International Association of Geomagnetism and Aeronomy (IAGA), Division V, Working Group 8, The 9th generation International Geomagnetic Reference Field, Earth Planets Space, Research News, 55, i-ii, 2003.
8) Kaiho, Y., N. Takahashi, T. Sato, G. Fujie, S. Kodaira, and Y. Kaneda, Wide-angle seismic profiling of oceanic island arc in the southern Izu-Ogasawara arc -KY0502 cruise-, JAMSTEC Rep. Res. Dev., 3, 43-52, 2006.
9) Kido, Y., Geophysical features of the north Izu-Ogasawara region, Chikyu, 52, 104-112, 2005.
10) Kodaira, S., T. Sato, N. Takahashi, A. Ito, Y. Tamura, Y. Tatsumi, and Y. Kaneda, Seismological evidence for growing and re-melting continental crust in the Izu-Bonin arc, Japan Geoscience Union Meeting, J239-005, 2006.
11) Koyama, M., S. M. Cisowski, and P. Pezard, Paleomagnetic evidence for northward drift and clockwise rotation of the Izu-Bonin forearc since the early Oligocene, In Taylor, B., Fujioka, K, et al., Proc. ODP, Sci. Results, 126, College Station, TX (Ocean Drilling Program), 353-370, 1992.
12) Kuo, B. Y. and D. W. Forsyth, Gravity anomalies of the ridge-transform system in the South Atlantic between 31° and 34.5°S: Upwelling centers and variations in crustal thickness, Mar. Geophys. Res., 10, 205-232, 1988.
13) Lin, J., G. M. Purdy, H. Schouten, J.-C. Sempéré, and C. Zervas, Evidence from gravity data for focused magmatic accretion along the Mid-Atlantic Ridge, Nature, 344, 627-632, 1990.
14) Miura, S., T. Sato, T. No, N. Takahashi, S. Kodaira, and Y. Kaneda, Wide-angle seismic experiment crossing the Sofu-gan tectonic line in the Izu-Ogasawara arc -KY0502 cruise-, JAMSTEC Rep. Res. Dev., 3, 19-29, 2006.
15) Nishizawa, A., K. Kaneda, A. Nakanishi, N. Takahashi, and S. Kodaira, Crustal structure of the ocean-island arc transition at the mid Izu-Ogasawara (Bonin) arc margin, Earth Planets Space, 58, e33-e36, 2006.
16) Park, J.-O., T. Tsuru, Y. Kido, M. K. Thu, S. Kodaira, and Y. Kaneda, Multichannel seismic reflection image across the Izu-Bonin island arc system -preliminary results-, Fall meeting, Seismo. Soc. Japan, P071, 222, 2002.
17) Press, W. H., S. A. Teukolsky, W. T. Vetterling, and B. P. Flannery, Numerical Recipes: The Art of Scientific Computing, Cambridge University Press, New York, 963 pp, 1992.
18) Prince, R. A. and D. W. Forsyth, Horizontal extent of anomalously thin crust near the Vema Fracture Zone from the three-dimensional analysis of gravity anomalies, J. Geophys. Res., 93, 8,051-8,063, 1988.
19) Tamura, Y., O. Ishizuka, H. Shukuno, H. Kawabata, K. Tani, T. Fujiwara, Y. Kido, and R. S. Fiske, Horeki backarc volcano of the Izu-Bonin arc, Japan Geoscience Union Meeting, J161-035, 2006.
20) Takahashi, N., S. Kodaira, T. Sato, A. Ito, T. No, and Y. Kaneda, Wide-angle seismic profiling of arc-arc collision zone in the northern Izu-Ogasawara arc -KY0408 cruise-, JAMSTEC Rep. Res. Dev., 1, 23-36, 2005.
21) Tsuru, T., J.-O. Park, T. No, K. Takizawa, and Y. Kaneda, Cruise report of 2004 seismic reflection surveys in Izu-Ogasawara Arc, JAMSTEC Rep. Res. Dev., 2, 1-12, 2005.
22) Ueda, Y., Magnetic and gravity field analyses of Izu-Ogasawara (Bonin) Arc and their tectonic implications, J. Geomag. Geoelectr., 48, 421-445, 1996.
23) Wessel, P. and W. H. F. Smith, New version of Generic Mapping Tools released, EOS Trans. AGU, 76, 329, 1995.
24) Yamazaki, T. and M. Yuasa, Possible Miocene rifting of the Izu-Ogasawara (Bonin) arc deduced from magnetic anomalies, Island Arc, 7, 374-382, 1998.

(Received July 14, 2006)